Part II
Tiny Technologies for Modulating Biological Systems

Micro- and Nanosystems for Biotechnology, First Edition. Edited by J. Christopher Love.

6
Nanotechnologies for the Bioelectronic Interface

Benjamin W. Avants, Hongkun Park, and Jacob T. Robinson

6.1
Introduction

Each second, the 80 billion neurons in the human brain send and receive many electrical impulses known as *spikes* or *action potentials*. To understand how these signals represent our perceptions, thoughts, and actions, scientists are seeking improved bioelectronic interfaces that can simultaneously detect and manipulate the activity of many individual neurons. With the tools available today, scientists can simultaneously record electrical activity from several hundred neurons at a time in the mammalian brain [1–3]. This number, however, is a tiny fraction of the tens of thousands of neurons thought to participate in computational tasks related to sensory perception and behavior.

To interact with greater numbers of cells, future bioelectronic interfaces must undergo radical technological advances. One promising approach utilizes nanotechnology borrowed from semiconductor manufacturing to create tiny bioelectronic interfaces that can increase the number of cells recorded during an experiment and improve the signal to noise ratio of these recordings. Nanotechnology is one of many emerging methods to record neural activity giving scientists more freedom in selecting methods that best meet the needs of their experiment. The main advantage of nanotechnology is the clear path toward large-scale high-temporal resolution measurements. Alternative approaches like voltage or calcium sensitive fluorescence enable scientists to identify specific cells and cell types responsible for recorded signals, but the response times of fluorescent molecules that can be used *in vivo* are typically several milliseconds [4–6] – much slower than the 10 kHz sampling rates of typical electrical probes. Electrical techniques can be improved without nanoscale integration. For example, automated patch-clamping robots can replace traditional manual electrophysiology [7], but without a chip-scale solution to hardware like micromanipulators, it is difficult to achieve the same parallelization possible with semiconductor nanofabrication. While any particular experiment may employ one or several different neural interfaces, we focus this chapter on recent demonstrations of nanodevices that

Micro- and Nanosystems for Biotechnology, First Edition. Edited by J. Christopher Love.

may provide the foundation for highly parallel minimally invasive bioelectronic interfaces. We also discuss the principles behind nanoscale bioelectronic interfaces and what may lie ahead for this technology.

6.2
Modeling the Bioelectronic Interface

The primary goal of many bioelectronic interfaces is to selectively record and control the transmembrane potential (V_m) of many neurons within the brain. To reach this goal, future interfaces should provide a *scalable* single-cell recording and stimulation technology, that is, each electrode should be easily reproduced over large areas to create a massively parallel interface to large numbers of cells. To understand how effective any potential electrode design may be, it useful to develop an equivalent circuit model and calculate the electronic coupling strength. This coupling strength describes the magnitude of the recorded signal compared to the true transmembrane potential (V_{out}/V_m).

The equivalent circuit model used by Zeck and Fromherz and later adapted by Hai *et al.*, and Robinson *et al.*, serves as a good approximation for calculating the electronic coupling strength of electrodes near the cell body [8–10]. We define the coupling strength for recording as the ratio of the measured voltage signal relative to the change in the transmembrane potential ($\Delta V_{out}/\Delta V_m$), and calculate this value using our equivalent circuit. To simplify the analysis we will not consider the roles of specific ion channels. Instead, we will combine all the ion channels in to a representative membrane resistance (R_m) and a reversal potential that is equal to the cell's resting membrane potential (V_{rest}) (Figure 6.1). We can

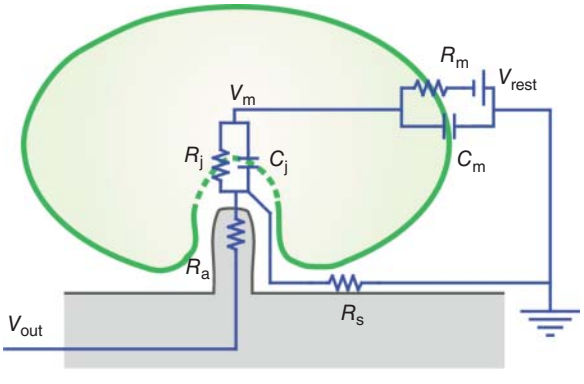

Figure 6.1 Equivalent circuit model of the bioelectronic interface. The measured potential (V_{out}) primarily depends upon the access resistance (R_a), the seal resistance (R_s), and the resistance and capacitance of the patch of membrane and the electrode junction (R_j and C_j, respectively). The membrane resistance (R_m) and capacitance (C_m) determine the membrane time constant. In the absence of an applied current the membrane potential (V_m) is equal to the resting potential (V_{rest}). Using this equivalent circuit model we can calculate the electronic coupling strength ($\Delta V_{out}/\Delta V_m$) and plot this value as a function of R_s and R_a as shown in Figure 6.2.

then model the patch of membrane covering the electrode as a having a junction resistance (R_j) and a junction capacitance (C_j). We can then simulate an action potential by driving V_{rest} with a typified action potential waveform and calculate the maximum $\Delta V_{out}/\Delta V_m$. Note that to simply illustrate the effects of the access and seal resistances we have ignored the many non-linear terms that affect real electrical interfaces. As a result, this model reproduces the qualitative effects of the seal and access resistances; however, the reader is encouraged to refer to the many papers on detailed modeling of the cell-electrode interface for a more complete model that includes the effect of the bath solution and the spatial extents of the neuron [11, 12]. These terms are necessary to reproduce the waveform of typical extracellular recordings [11, 12].

With our equivalent circuit model we can now plot $\Delta V_{out}/\Delta V_m$ as a function of R_s and R_a to reveal three qualitatively different coupling regimes that we refer to as: (i) Extra-cellular, (ii) Intra-cellular, and (iii) In-cell (Figure 6.2). We discuss the

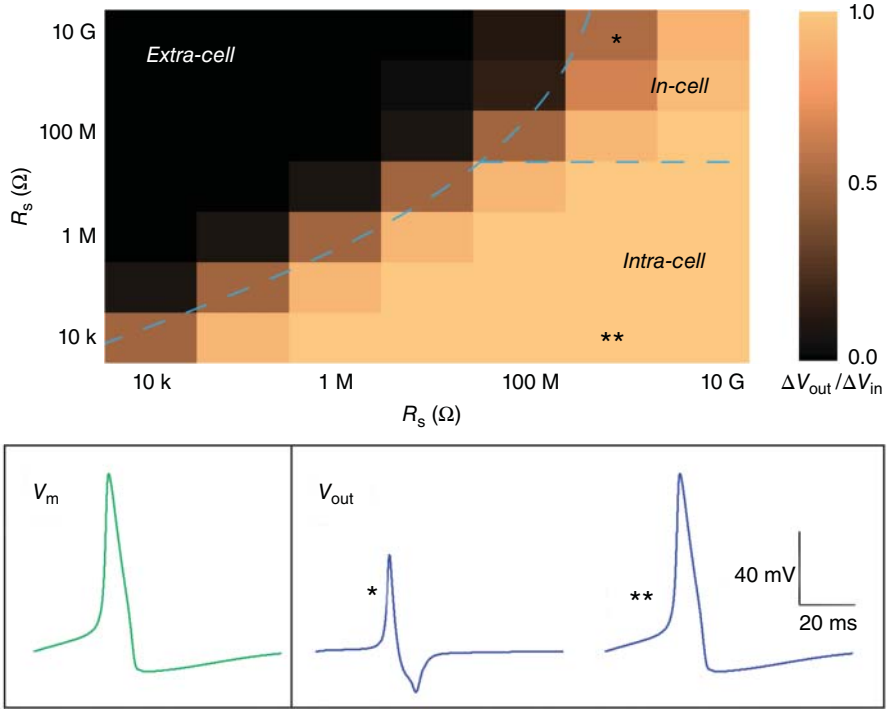

Figure 6.2 Electronic coupling regimes. Calculating the voltage during a simulated action potential using the equivalent circuit model in Figure 6.1 allows us to plot the coupling strength ($\Delta V_{out}/\Delta V_m$) as a function of R_a and R_s. This plot reveals extra-, intra-, and in-cell regimes divided roughly by the dashed lines in the upper figure. The input action potential waveform is shown on the bottom left (green) while typical In-cell and Intra-cell recorded waveforms are shown at the bottom right (* and **, respectively). These voltage waveforms correspond to * and ** labeled regions in the upper plot.

technologies associated with these different recording regimes and their advantages and disadvantages in the sections below. Note that Figure 6.2 is intended to be a qualitative representation of the three different coupling regimes. The exact coupling coefficients and locations of the coupling regimes in this parameter space depend on the component values used in the equivalent circuit model, which will vary based on the properties of both the cell and the electrode.

6.3 Experimental Approaches for Extra-Cellular Coupling

Extra-cellular coupling describes most nanoscale bioelectronic interfaces including most multielectrode arrays (MEAs) based on metallic electrodes [13], field effect transistors (FETs) [14–16], implanted wires [17, 18], and multielectrode probes [19, 20] (Figure 6.3). In the extra-cellular regime the cell membrane remains intact (R_a is large) and the seal resistance between the electrode and the cell membrane is low. The signal recorded by the electrode is therefore dominated

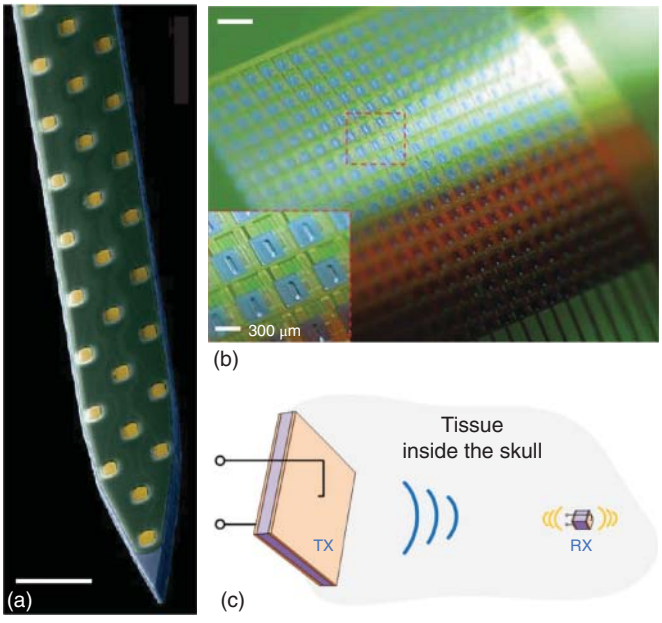

Figure 6.3 Nanofabricated extra-cellular electrodes. (a) A silicon shank containing dozens of electrodes over a 1.3 mm length can record from many depths when inserted into neural tissue [20]. © J. Du, with permission. (b) Flexible electrodes and multiplexers imbedded in PDMS can conform to the surface of the brain for high-density ECoG [21]. © Nature Publishing Group (2011), with permission. (c) Free-floating electrodes may be addressable within neural tissue using ultrasound as a route for tether-less "neural dust." Adapted from Ref. [22], © Seo. Scale bars: (a) 50 µm and (b) 1 mm.

by the voltage drop that results from ionic currents flowing into and out of the cell membrane. From Ohm's law it can be shown that this current is proportional to dV_m/dt. Therefore the waveform measured in the extra-cellular regime typically resembles the first derivative of an action potential and is significantly attenuated [11, 12]. For example, single unit recordings using extracellular electrodes typically report peak extra-cellular voltages less than 1 mV compared to the roughly 100 mV change in V_m that accompanies a typical action potential. Note that while the exact shape of the extracellular waveform is not produced in our simplified equivalent circuit model, the amplitude of the response is similar to those reported in literature. To reproduce the shape of the extracellular waveform one must include the spatial extents of the neuron and/or the properties of ionic diffusion in the surrounding media [11, 12].

One of the main reasons that extra-cellular measurements are the dominant form of nanoscale bioelectronic interfaces is the relative ease of establishing an extra-cellular recording configuration. For example, culturing neurons on top of an array of flat electrodes typically establishes extra-cellular coupling with neurons on top of the electrode [13–16]. Similarly, thin wires and multi-electrode probes can often establish extra-cellular coupling when implanted into the brain [17, 18].

One of the major disadvantages of extracellular recordings, however, is that the severely attenuated signals prevent measurement of post-synaptic potentials that are typically 20–100 times weaker than an action potential. While the small membrane fluctuations that result from synaptic input is often not sufficient to generate an action potential, this so-called sub-threshold activity is critical for measuring synaptic strengths and how these strengths change over time. This changing synaptic strength (referred to as *plasticity*) is believed to be a critical component of learning and memory and is therefore a critical quantity for many neuroscience experiments [23, 24]. To measure sub-threshold activity scientists typically turn to intra-cellular or in-cell recording configurations.

6.4 State-of-the-Art Extra-Cellular Nanoscale Interfaces

Although extra-cellular recordings typically have low signal to noise ratios they are nevertheless the most common type of *in vivo* bioelectronic interface. Recognizing the importance of extra-cellular recordings, scientists and engineers are developing improved extra-cellular bioelectronic interfaces using nanofabrication technology. The key advantages of new nanofabricated extra-cellular electrodes are improved electrode density and flexible substrates. For example, ultra-high-density electrodes in silicon now feature dozens of electrodes along a single shank only 1.3 mm long [20] (Figure 6.3a). To reduce the damage caused by the probe and improve the longevity of the measurement scientists are also developing electrodes on flexible substrates. Viventi *et al.* have used recent developments in flexible silicon electronics [25] to create nanofabricated Pt

electrodes and silicon multiplexers embedded in flexible polydimethylsiloxane (PDMS) that can conform to the surface of the brain and improve the density of electro-cortical encephalography (ECoG) [21] (Figure 6.3b). Similarly, nanowire (NW) FETs can be incorporated into flexible SU-8 scaffolds that can be rolled and used for 3D tissue culture [26]. These scaffolds can even be injected through a syringe into the brain where they can unfold into a flexible mesh that can record neuronal activity *in vivo* [27]. This idea of injectable neural interfaces has also been demonstrated with microscale light emitting diodes (LEDs) on flexible substrates [28]. These LEDs can then modulate brain activity by activating neurons that express a light-gated ion channel like channelrhodopsin [29]. These early demonstrations of injectable, flexible neural interfaces point toward implantation procedures with reduced risk and long-term, stable neural recordings.

Future extra-cellular electrodes may dispense of substrates all together. A recent proposal by Seo *et al.* has suggested that free-floating electrodes (also known as "Neural Dust") could be injected into the brain and addressed using a wireless ultrasound interrogator placed on the surface of the brain [22] (Figure 6.3c). This interrogator could then communicate through the skull to a transceiver. In this way, the skull can be completely closed following the electrode insertion improving the longevity of the interface by reducing the risk of bacterial infections [22]. One potential challenge for silicon nanodevices for neural interfaces is the fact that silicon has been shown to slowly dissolve under physiological conditions [30]. One can take advantage of this fact and develop transient neural interfaces that operate for a pre-determined period time determined before being absorbed by the body [30]. To maintain long-term neural recording with silicon nanodevices, it is possible to coat the silicon surface with a protective water barrier like $HfO_2 - Al_2O_3$ laminates that have been shown to protect NW functionality for over a year under physiological conditions [31]. Whatever the future of extra-cellular electrodes may be, it is clear that nanofabrication offers opportunities for improved device characteristics, densities, and flexibility.

6.5 Experimental Approaches for Intra-Cellular Coupling

From the equivalent circuit analysis, it is clear that decreasing the access resistance and/or increasing the seal resistance significantly improves the coupling strength compared to the extra-cellular regime. When this improved coupling is the result of decreased access resistance it is known as *intra-cellular coupling*. This configuration is similar to the whole-cell patch or sharp electrode measurements performed using glass micropipettes [32].

Early attempts to integrate patch clamp electrophysiology on a chip mainly relied on creating micron scale hole arrays either in the substrate of a cell enclosure [33–43] (so called planar-patch clamp array) or in the walls of microfabricated chambers [44, 45]. These approaches are mainly successful for clonal cells in suspension like oocytes, Human Embryonic Kidney (HEK) cells, and

Chinese Hamsters Ovary (CHO) cells [43]. As a result, planar patch clamp tools are primarily used to screen pharmacological compounds [43], and are not used to investigate neural circuit or cardiac activity that necessitates the growth of an adherent cell community.

6.6 State-of-the-Art Intra-Cellular Nanoscale Interfaces

Recently, alternatives to planar patch technology has been developed that can record from neural and cardiac tissue. This technology is based on vertical NW arrays that can access the interior of living cells [46–53]. Unlike traditional micropipettes and planar patch clamp arrays, NW electrodes do not use suction or mechanical pressure to rupture the cellular membrane. Instead, NW electrodes can penetrate the cellular membrane by spontaneous internalization [10, 54–56] or by electroporation [57, 58] (Figure 6.4).

While the mechanism of spontaneous internalization that allows a NW to penetrate the cellular membrane is not fully understood, studies suggest this may be a rare process that accompanies cell adhesion to a surface. In one study, Xu *et al.* reported that between 7% and 11% of vertical nanostraws penetrate the membrane of CHO cells after they adhere to the surface [59]. The authors also showed that the percentage of nanostraws penetrating the cell membrane could be improved by promoting cell adhesion through surface functionalization [59]. These results are consistent with reports that biomolecules decorating the surface of vertical NWs are transferred into the cytoplasm of cells that adhere to NW-studded substrates [50–52]. Alternative surface treatments may promote more effective NW penetration. Tian *et al.* [54] and subsequent work [55, 56, 60] has shown that the NW internalization can be facilitated by surface functionalization using a phospholipid, and Almquist and Melosh has shown that it is possible to reduce the force required to embed a probe in the lipid bilayer by engineering the hydrophobicity of the NW surface [61, 62]. Interestingly, no clear evidence of NW cell penetration was observed when cells were imaged using transmission electron microscopy (TEM) after the cells were fixed, stained, and sectioned [63]. However, it is important to note that the significant differences in the experimental preparations makes comparisons between these results difficult to interpret. For instance, the cell types, surface treatment, and time spent on the NW substrate varied across these experiments making it difficult to compare studies of NW penetration.

As an alternative to spontaneous cell internalization Xie *et al.* [57] and Robinson *et al.* [10] showed that a brief voltage pulse or constant current flux can reduce the junction membrane resistance and achieve an intra-cellular coupling configuration. Xie *et al.* have shown that the intracellular coupling strength achieved by electroporation decreases over time as the cell membrane repairs itself [57]. With vertical NW electrodes, the cell membrane repairs itself after approximately 10 min [57]. Subsequent voltage pulses can restore the intra-cellular coupling and

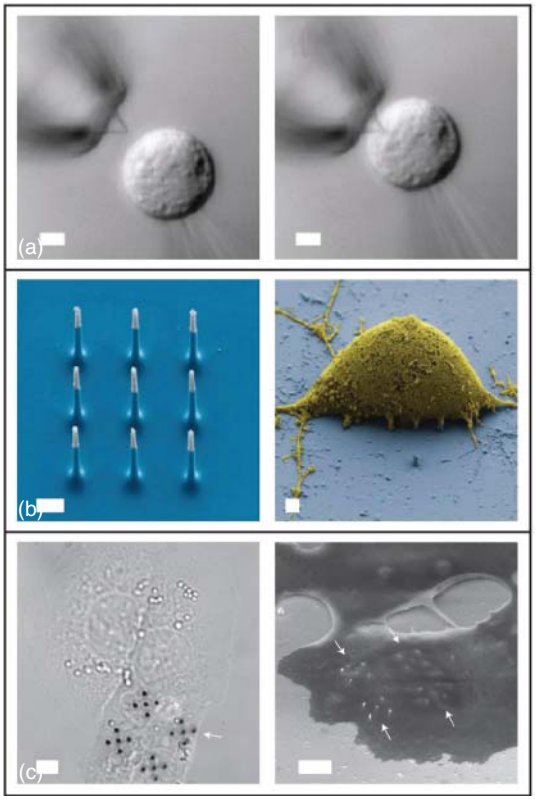

Figure 6.4 Nanofabricated intra-cellular electrodes. (a) A kinked NW FET can be inserted into an HL-1 cell to record V_m. Adapted from Ref. [54]. (b) Arrays of vertical NW electrodes can penetrate the cell membrane of primary neurons to both record and stimulate action potentials in cells grown directly on the silicon substrate [10]. © J. Robinson. (c) Arrays for vertical NW electrodes can also record action potentials from inside cardiac cells grown on the NW substrate. Adapted from Ref. [57], NCBI. Scale bars: (a) 5 μm, (b) 1 μm, and (c) 5 μm.

this process can be repeated over several days [57]. Extended coupling times have recently been reported by Lin *et al.* showing that hollow nanotubes can maintain intracellular coupling for nearly an hour following electroporation [58].

The major advantage of the nanoscale intra-cellular electrodes like those discussed in this section is the combination of improved signal to noise ratio compared to extra-cellular methods and scalable fabrication compared to conventional intra-cellular electrodes based on micropipettes. Because conventional micropipette electrodes require discrete macroscale components like amplifying headstages and micromanipulators contemporary patch clamp electrophysiology is typically limited to only a few simultaneous measurements. The vision for nanofabricated bioelectronics interfaces is that silicon nanofabrication procedures will mass-produce devices with hundreds of thousands of recording

sites on a single monolithic platform. Compared to extra-cellular electrode arrays, we expect arrays of intra-cellular electrodes to record both action potentials and sub-threshold activity allowing scientists to monitor synaptic input and synaptic strengths as they evolve over time.

For intra-cellular nanoelectrodes to reach their full potential, additional work is needed to improve their electrical performance and the stability of the interface. While successive electroporation events can regain an intra-cellular configuration, repeated electroporation may have adverse effects on cell health. Ideally an intra-cellular electrode would maintain a stable coupling coefficient for several days allowing scientists to monitor subtle changes in the electrophysiology and synaptic activity. Improved coupling stability may be possible through proper surface modifications like those proposed by Almquist and Melosh [61, 62] or the lipophilic coating used by Tian *et al.* and others [54–56, 60]. Many of these surface treatments, however, would prevent cells from growing directly on the substrate or may be unstable *in vivo.* More work is needed to develop surface treatments appropriate for long-term studies *in vivo.*

6.7 Experimental Approaches for In-Cell Coupling

As an alternative to intra-cellular coupling, the coupling strength can also be improved by increasing the seal resistance between the electrode and the cell membrane. In this regime, although the cell membrane remains intact, the electrode is tightly sealed to the cell membrane and can accurately track the transmembrane potential. This coupling configuration has been described as "in-cell" recording by Hai *et al.*, and has been achieved by culturing cells on top of gold mushroom-shaped electrodes (Figure 6.5) [9, 64–67]. To further improve the seal between the electrode and the cell, the authors coated the gold surface with a peptide that promotes macrophagocytosis. Although the electrode does not penetrate the cellular membrane, the capacitive coupling between the electrode and the interior of the cell produces recordings that resemble intra-cellular recording of the membrane potential. The waveform shown in Figure 6.2* shows an example of the "in-cell" type waveforms as computed from our equivalent circuit model. The notable difference between these waveforms and the intracellular waveforms is the exaggerated after-hyperpolarization. This artifact however, can be corrected by deconvolving the waveform with the impulse response of the electrode. The result of this deconvolution yields a waveform that is equivalent to intracellular measurements [64]. Although the equivalent circuit model of the in-cell configuration reproduces the experimentally measured waveform, the strength of this electronic coupling is not entirely understood. Most notably, the equivalent circuit model that best reproduces the measured waveforms requires a membrane resistance approximately 10 times lower than what has typically been reported. It is possible that small pores in the membrane may increase the cell membrane conductivity however transmission electron microscope images

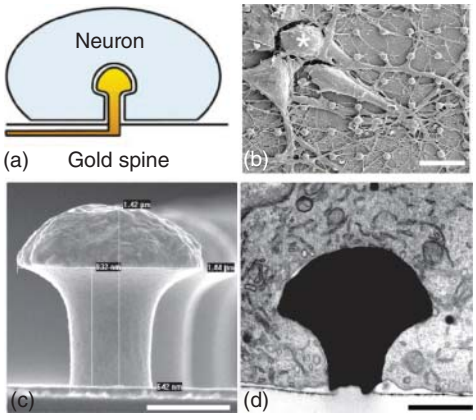

Figure 6.5 In-cell electrodes. (a) Schematic of the in-cell recording configuration. Adapted from Ref. [64], with permission from the Nature Publishing Group 2010. (b) Scanning electron micrograph of rat neurons cultured on top of a gold mushroom electrode array. Adapted from Ref. [65], NCBI. (c) Scanning electron micrograph of the profile of a gold mushroom electrode. (d) Transmission electron micrograph of interface between an *Aplysia* neuron and the gold mushroom electrode. Panels (c) and (d) Adapted from Ref. [9], NCBI. Scale bars: (b) 12 µm, (c) 0.5 µm, and (d) 0.5 µm.

suggest that the membrane remains intact (Figure 6.5d and [64]). To explain their measurements, Hai *et al.* propose that recruitment of ion channels to the membrane encapsulation site locally increases the membrane conductance [9]. This hypothesis, however, has yet to be tested.

The major advantage of in-cell measurements is that the coupling strength remains stable (as compared to an electroporated interface) and the membrane remains intact allowing the cells to survive for days in the recording configuration. It is important to note that to date, in-cell recordings have only been reported for *Aplysia* neurons that are approximately 10 times larger than typical mammalian neurons. Additional challenges may face the adaptation of technology for the smaller and more fragile mammalian neurons.

6.8 Outlook

Nanofabricated bioelectronic interfaces offer many opportunities to improve recording and stimulation of the brain. Mainly the small size and high-aspect ratios of nanodevices can improve the density and fidelity of neural recordings. Applications for this technology range from basic neuroscience research, to therapies like deep brain stimulation, to brain machine interfaces. Of course, *in vivo* applications of intra-cellular and in-cell electrodes require more experiments to show that the same cell-electrode interfaces can be developed *in vivo.* Likely approaches for these demonstrations include electrode shanks that feature

mushroom or NW electrodes that protrude from the surface. Additionally, nanofabricated bioelectronic interfaces may find applications in lab-on-a-chip technologies where NW electrodes could rapidly record the electrical activity of cells before they are sorted into populations according to their electrophysiology.

While the future of nanofabricated bioelectronic interfaces remains bright, more work is needed for these interfaces to reach their potential. Namely, these devices need to be mass-produced so that they can be adopted in laboratory and clinical settings. Furthermore, the physical and electrochemical interface between the cell and the nanostructures must be better understood and controlled. For manufacturing, it is likely that fabrication processes that most resemble conventional semiconductor manufacturing will lead to the first widely distributed devices; however, some nanodevices that rely on non-conventional fabrication may have performance advantages that justify future mass-production in specialized facilities.

Overall, as semiconductor manufacturing technologies are applied to bioelectronic interfaces we will likely witness great improvements in our ability to monitor and control the electrical activities of individual cells. Like gene sequencing, where major advancements resulted from collaborations between nanotechnologists, engineers, and biologists, it is our vision applying nanotechnology to bioelectronic interfaces will catalyze similar rapid technological advances yielding fundamental biological insights and improved strategies for treating disease.

References

1. Marblestone, A.H. *et al.* (2013) Physical principles for scalable neural recording. *Front. Comput. Neurosci.*, **7**, 137.
2. Cotton, R.J., Froudarakis, E., Storer, P., Saggau, P., and Tolias, A.S. (2013) Three-dimensional mapping of microcircuit correlation structure. *Front. Neural Circuits*, **7**, 151.
3. Schwarz, D.A. *et al.* (2014) Chronic, wireless recordings of large-scale brain activity in freely moving rhesus monkeys. *Nat. Methods*, **11**, 670–676.
4. Tian, L. *et al.* (2009) Imaging neural activity in worms, flies and mice with improved GCaMP calcium indicators. *Nat. Methods*, **6**, 875–881.
5. Chen, T.-W. *et al.* (2013) Ultrasensitive fluorescent proteins for imaging neuronal activity. *Nature*, **499**, 295–300.
6. Ahrens, M., Orger, M., Robson, D., Li, J., and Keller, P. (2013) Whole-brain functional imaging at cellular resolution using light-sheet microscopy. *Nat. Methods*, **10**, 413.
7. Kodandaramaiah, S. and Franzesi, G. (2012) Automated whole-cell patch-clamp electrophysiology of neurons in vivo. *Nat. Methods*, **9**, 585.
8. Zeck, G. and Fromherz, P. (2001) Noninvasive neuroelectronic interfacing with synaptically connected snail neurons immobilized on a semiconductor chip. *Proc. Natl. Acad. Sci. U.S.A.*, **98**, 10457–10462.
9. Hai, A., Shappir, J., and Spira, M.E. (2010) Long-term, multisite, parallel, in-cell recording and stimulation by an array of extracellular microelectrodes. *J. Neurophysiol.*, **104**, 559–568.
10. Robinson, J.T. *et al.* (2012) Vertical nanowire electrode arrays as a scalable platform for intracellular interfacing to neuronal circuits. *Nat. Nanotechnol.*, **7**, 180–184.
11. Bédard, C., Kröger, H., and Destexhe, A. (2004) Modeling extracellular field potentials and the frequency-filtering properties of extracellular space. *Biophys. J.*, **86**, 1829–1842.

12. Gold, C., Henze, D.A., Koch, C., and Buzsáki, G. (2006) On the origin of the extracellular action potential waveform: a modeling study. *J. Neurophysiol.*, **95**, 3113–3128.
13. Pine, J. (2006) *Advances in Network Electrophysiology*, Springer, pp. 3–23.
14. Voelker, M. and Fromherz, P. (2005) Signal transmission from individual mammalian nerve cell to field-effect transistor. *Small*, **1**, 206–210.
15. Fromherz, P. (2002) Electrical interfacing of nerve cells and semiconductor chips. *ChemPhysChem*, **3**, 276–284.
16. Eversmann, B. *et al.* (2003) A 128 × 128 CMOS biosensor array for extracellular recording of neural activity. *IEEE J. Solid-State Circuits*, **38**, 2306–2317.
17. McNaughton, B.L., O'Keefe, J., and Barnes, C.A. (1983) The stereotrode: a new technique for simultaneous isolation of several single units in the central nervous system from multiple unit records. *J. Neurosci. Methods*, **8**, 391–397.
18. Nicolelis, M.A. *et al.* (2003) Chronic, multisite, multielectrode recordings in macaque monkeys. *Proc. Natl. Acad. Sci. U.S.A.*, **100**, 11041–11046.
19. Maynard, E.M., Nordhausen, C.T., and Normann, R.A. (1997) The Utah intracortical electrode array: a recording structure for potential brain-computer interfaces. *Electroencephalogr. Clin. Neurophysiol.*, **102**, 228–239.
20. Du, J., Blanche, T.J., Harrison, R.R., Lester, H.A., and Masmanidis, S.C. (2011) Multiplexed, high density electrophysiology with nanofabricated neural probes. *PLoS One*, **6**, e26204.
21. Viventi, J. *et al.* (2011) Flexible, foldable, actively multiplexed, high-density electrode array for mapping brain activity in vivo. *Nat. Neurosci.*, **14**, 1599–1605.
22. Seo, D., Carmena, J.M., Rabaey, J.M., Alon, E., and Maharbiz, M.M. (2013) Neural Dust: An Ultrasonic, Low Power Solution for Chronic Brain-Machine Interfaces. arXiv:1307.2196 [q-bio.NC].
23. Chen, C. and Tonegawa, S. (1997) Molecular genetic analysis of synaptic plasticity, activity-dependent neural development, learning, and memory in the mammalian brain. *Annu. Rev. Neurosci.*, **20**, 157–184.
24. Martin, S.J., Grimwood, P.D., and Morris, R.G. (2000) Synaptic plasticity and memory: an evaluation of the hypothesis. *Annu. Rev. Neurosci.*, **23**, 649–711.
25. Viventi, J. *et al.* (2010) A conformal, bio-interfaced class of silicon electronics for mapping cardiac electrophysiology. *Sci. Transl. Med.*, **2**, 24ra22.
26. Tian, B. *et al.* (2012) Macroporous nanowire nanoelectronic scaffolds for synthetic tissues. *Nat. Mater.*, **11**, 1–9.
27. Liu, J. *et al.* (2015) Syringe-injectable electronics. *Nat. Nanotechnol.*, **10**, 629–636.
28. Kim, T.-I. *et al.* (2013) Injectable, cellular-scale optoelectronics with applications for wireless optogenetics. *Science*, **340**, 211–216.
29. Yizhar, O., Fenno, L.E., Davidson, T.J., Mogri, M., and Deisseroth, K. (2011) Optogenetics in neural systems. *Neuron*, **71**, 9–34.
30. Hwang, S.-W. *et al.* (2012) A physically transient form of silicon electronics. *Science*, **337**, 1640–1644.
31. Zhou, W. *et al.* (2014) Long term stability of nanowire nanoelectronics in physiological environments. *Nano Lett.*, **14**, 1614–1619.
32. Molleman, A. (2003) *Patch Clamping*, John Wiley & Sons, Ltd.
33. Klemic, K.G., Klemic, J.F., Reed, M.A., and Sigworth, F.J. (2002) Micromolded PDMS planar electrode allows patch clamp electrical recordings from cells. *Biosens. Bioelectron.*, **17**, 597–604.
34. Fertig, N., Blick, R.H., and Behrends, J.C. (2002) Whole cell patch clamp recording performed on a planar glass chip. *Biophys. J.*, **82**, 3056–3062.
35. Wang, X. and Li, M. (2003) Automated electrophysiology: high throughput of art. *Assay Drug Dev. Technol.*, **1**, 695–708.
36. Pantoja, R. *et al.* (2004) Silicon chip-based patch-clamp electrodes integrated with PDMS microfluidics. *Biosens. Bioelectron.*, **20**, 509–517.
37. Sigworth, F.J. and Klemic, K.G. (2005) Microchip technology in ion-channel research. *IEEE Trans. Nanobiosci.*, **4**, 121–127.

38. Chen, C. and Folch, A. (2006) A high-performance elastomeric patch clamp chip. *Lab Chip*, **6**, 1338–1345.
39. Brüggemann, A., Stoelzle, S., George, M., Behrends, J.C., and Fertig, N. (2006) Microchip technology for automated and parallel patch-clamp recording. *Small*, **2**, 840–846.
40. Li, X., Klemic, K.G., Reed, M.A., and Sigworth, F.J. (2006) Microfluidic system for planar patch clamp electrode arrays. *Nano Lett.*, **6**, 815–819.
41. Matthews, B. and Judy, J.W. (2006) Design and fabrication of a micromachined planar patch-clamp substrate with integrated microfluidics for single-cell measurements. *J. Microelectromech. Syst.*, **15**, 214–222.
42. Dunlop, J., Bowlby, M., Peri, R., Vasilyev, D., and Arias, R. (2008) High-throughput electrophysiology: an emerging paradigm for ion-channel screening and physiology. *Nat. Rev. Drug Discovery*, **7**, 358–368.
43. Brüggemann, A. *et al.* (2008) Planar patch clamp: advances in electrophysiology. *Methods Mol. Biol.*, **491**, 165–176.
44. Ionescu-zanetti, C. *et al.* (2005) Mammalian electrophysiology on a microfluidic platform. *Proc. Natl. Acad. Sci. U.S.A.*, **102**, 9112–9117.
45. Lau, A.Y., Hung, P.J., Wu, A.R., and Lee, L.P. (2006) Open-access microfluidic patch-clamp array with raised lateral cell trapping sites. *Lab Chip*, **6**, 1510–1515.
46. Turner, A.M.P. *et al.* (2000) Attachment of astroglial cells to microfabricated pillar arrays of different geometries. *J. Biomed. Mater. Res.*, **51**, 430–441.
47. Hällström, W. *et al.* (2007) Gallium phosphide nanowires as a substrate for cultured neurons. *Nano Lett.*, **7**, 2960–2965.
48. Jiang, K. *et al.* (2009) Medicinal surface modification of silicon nanowires: impact on calcification and stromal cell proliferation. *ACS Appl. Mater. Interfaces*, **1**, 266–269.
49. Qi, S., Yi, C., Ji, S., Fong, C.-C., and Yang, M. (2009) Cell adhesion and spreading behavior on vertically aligned silicon nanowire arrays. *ACS Appl. Mater. Interfaces*, **1**, 30–34.
50. Shalek, A.K. *et al.* (2010) Vertical silicon nanowires as a universal platform for delivering biomolecules into living cells. *Proc. Natl. Acad. Sci. U.S.A.*, **107**, 1870–1875.
51. Chevrier, N. *et al.* (2011) Systematic discovery of TLR signaling components delineates viral-sensing circuits. *Cell*, **147**, 853–867.
52. Shalek, A.K. *et al.* (2012) Nanowire-mediated delivery enables functional interrogation of primary immune cells: application to the analysis of chronic lymphocytic leukemia. *Nano Lett.*, **12**, 6498–6504.
53. Na, Y.-R. *et al.* (2013) Probing enzymatic activity inside living cells using a nanowire-cell 'sandwich' assay. *Nano Lett.*, **13**, 153–158.
54. Tian, B. *et al.* (2010) Three-dimensional, flexible nanoscale field-effect transistors as localized bioprobes. *Science*, **329**, 830–834.
55. Duan, X. *et al.* (2012) Intracellular recordings of action potentials by an extracellular nanoscale field-effect transistor. *Nat. Nanotechnol.*, **7**, 174–179.
56. Qing, Q. *et al.* (2014) Free-standing kinked nanowire transistor probes for targeted intracellular recording in three dimensions. *Nat. Nanotechnol.*, **9**, 142–147.
57. Xie, C., Lin, Z., Hanson, L., Cui, Y., and Cui, B. (2012) Intracellular recording of action potentials by nanopillar electroporation. *Nat. Nanotechnol.*, **7**, 185–190.
58. Lin, Z.C., Xie, C., Osakada, Y., Cui, Y., and Cui, B. (2014) Iridium oxide nanotube electrodes for sensitive and prolonged intracellular measurement of action potentials. *Nat. Commun.*, **5**, 1–10.
59. Vandersarl, J.J., Xu, A.M., and Melosh, N.A. (2012) Nanostraws for direct fluidic intracellular access. *Nano Lett.*, **12**, 3881–3886.
60. Fu, T.-M. *et al.* (2014) Sub-10-nm intracellular bioelectronic probes from nanowire-nanotube heterostructures. *Proc. Natl. Acad. Sci. U.S.A.*, **111**, 1259–1264.
61. Almquist, B. and Melosh, N. (2010) Fusion of biomimetic stealth probes into

lipid bilayer cores. *Proc. Natl. Acad. Sci. U.S.A.*, **107**, 5815–5820.
62. Almquist, B.D. and Melosh, N.A. (2011) Molecular structure influences the stability of membrane penetrating biointerfaces. *Nano Lett.*, **11**, 2066–2070.
63. Hanson, L., Lin, Z.C., Xie, C., Cui, Y., and Cui, B. (2012) Characterization of the cell-nanopillar interface by transmission electron microscopy. *Nano Lett.*, **12**, 5815–5820.
64. Hai, A., Shappir, J., and Spira, M.E. (2010) In-cell recordings by extracellular microelectrodes. *Nat. Methods*, **7**, 200–202.
65. Fendyur, A., Mazurski, N., Shappir, J., and Spira, M.E. (2011) Formation of essential ultrastructural interface between cultured hippocampal cells and gold mushroom-shaped MEA- toward 'in-cell' recordings from vertebrate neurons. *Front. Neuroeng*, **4**, 14.
66. Hai, A. *et al.* (2009) Spine-shaped gold protrusions improve the adherence and electrical coupling of neurons with the surface of micro-electronic devices. *J. R. Soc. Interface*, **6**, 1153–1165.
67. Fendyur, A. and Spira, M.E. (2012) Toward on-chip, in-cell recordings from cultured cardiomyocytes by arrays of gold mushroom-shaped microelectrodes. *Front. Neuroeng*, **5**, 21.